

Valence excitation of NO₂ by impulsive stimulated x-ray Raman scattering

Daniel J. Haxton¹

¹*Department of Physics, University of California, Berkeley CA 94720*

Impulsive x-ray Raman excitations are the components of multidimensional x-ray spectroscopies that have been proposed. However the question of the optimum laser parameters to use for these impulsive excitations is still open. The multiconfiguration time-dependent Hartree-Fock (MCTDHF) method includes a description of the wave function that makes no assumptions about the degree of excitation, correlation, or ionization of the wave function. Impulsive x-ray Raman valence excitations of the NO₂ molecule driven by 1fs pulses tuned below the Oxygen K-edge were calculated in the fixed-nuclei approximation using the MCTDHF method. Fixing the duration but varying the central frequency and intensity of the pulse, not considering chirp, maximum population transfer is obtained at an intensity of approximately $3 \times 10^{17} \text{ W cm}^{-2}$, with the central frequency substantially 8eV red-detuned from the 2nd order optimum, and most likely driven by nonresonant Raman with the Oxygen K-edge continuum. Strong nonlinear effects are present at $10^{16} \text{ W cm}^{-2}$. The results will hopefully help guide the selection of experimental conditions under which multidimensional X-ray spectroscopies are most viable.

PACS numbers: 33.20.Fb 33.20.Rm 42.65.Re 42.65.Dr

I. INTRODUCTION

Recent proposals for using ultrafast x-ray pulses to study valence electron and hole motion in molecules [1, 2] rely on the creation of a coherent valence electronic wavepacket using two-photon, Raman transitions. Ultrafast, even attosecond broadband x-ray pulses drive the impulsive stimulated Raman process, the excitation via the pump frequencies and the stimulated emission of Stokes frequencies, leading to a coherent valence electronic excitation. The 1D- and 2D-SXRS multidimensional spectroscopies [1, 2] employ multiple impulsive Raman excitations in order to obtain information about electronic structure and couplings and the internuclear geometry. There have been several sophisticated theoretical and computational studies of multidimensional X-ray spectroscopic and related methods including Refs. [3–5].

However, these studies have often concentrated on electronic excitations to metastable core-excited states and neglected the continuum above the edge [6], and often they have explicitly computed the n th-order signal without considering large-magnitude higher-order behavior that might overwhelm lower orders even at low intensity. It is desirable to test the efficiency of impulsive stimulated x-ray Raman transitions in polyatomic molecules, in a fully nonperturbative, first-principles calculation that accounts for all the fundamental effects including multiple ionization, stark shifts, and highly correlated electronic dynamics. X-ray Raman transitions involve correlation of many electrons, because the excitation of the inner, core electrons affects the field experienced by the other electrons, and because the Auger decay of the intermediate states involves transitions of two electrons or more. Furthermore, testing the efficiency of the process at high intensity requires a method that accounts for the possibility of multiple electron transitions including those of core electrons.

The Multiconfiguration time-dependent Hartree-Fock

(MCTDHF) method is capable of calculating arbitrary nonperturbative quantum dynamics of electrons in medium-sized molecules, with all electrons active and able to be ionized. We have applied our implementation of MCTDHF [7–10] to predict transfer of population to valence excited electronic states due to stimulated X-ray transitions in the NO₂ molecule, in the fixed-nuclei approximation.

These MCTDHF calculations test the viability of impulsive Raman transitions for driving valence electronic state population transfer without making any assumptions about the degree of electronic excitation, correlation, or ionization, nor about the number of photons absorbed and emitted. The main approximations in these calculations are the omission of nuclear motion, the discretization via sinc functions, and the omission of relativistic (broadly speaking, non-dipole) effects. The results for population transfer with fixed nuclei should closely correspond to the physical result for electronic state population transfer, since the nitrogen and oxygen atoms are expected to move very little over the one-femtosecond duration of the pulse. We argue that the error due to discretization is likely small because the absorption cross sections above and below edge are accurately reproduced. At the limits of intensity, non-dipole effects may become significant and future work will examine their effect on impulsive Raman transitions.

We show that in the NO₂ molecule, for impulsive stimulated x-ray Raman scattering using 1fs pulses, transitions to the ²B₁ valence electronic state dominate. Population transfer of about 10^{-3} (a 3% coherence) may be driven at 2nd order by tuning below the near-edge fine structure, as in Ref. [6]. However, nonlinear effects quickly set in above $10^{16} \text{ W cm}^{-2}$, and a global optimization of population transfer as a function of intensity and central frequencies occurs with significant red detuning and appears to be driven by nonresonant Raman transitions through the continuum above-edge.

II. MCTDHF CALCULATION OF NO₂

Our implementation of MCTDHF [10] for electrons in molecules has already been described [7–9]. Briefly, the MCTDHF method [11–25] solves the time-dependent Schrödinger equation using a time-dependent linear combination of Slater determinants, with time-dependent orbitals in the Slater determinants. The nonlinear working equations are obtained through application of the Lagrangian variational principle [26, 27] to this wave function ansatz.

The representation of orbitals using sinc basis functions is described in Ref. [9]. For NO₂, we use a grid of $55 \times 55 \times 55$ (=166375) product sinc basis functions for the orbitals. The spacing between the functions is 0.2975614 bohr (about 0.56 Angstrom). The calculations are performed with full configuration interaction, 23 electrons in 15 orbitals, giving 621075 Slater determinants which are contracted to 305760 spin-adapted linear combinations and distributed among processors. The mean field time step was 0.02 atomic time units (approximately one half attosecond).

Complex coordinate scaling and stretching [28] is applied starting at ± 4 bohr in the x , y , and z directions. We perform the smooth complex scaling transformation upon the kinetic energy and derivative operators only. Lacking a viable method for defining the transformed two-electron operator, we do not transform the Coulomb operators. (We have found that this approximation, neglecting to transform the Coulomb operators, gives sharp ionization edges with truncated Rydberg series.) The complex ray is defined as

$$\begin{aligned} X(x) &= x + a(x - x_0) + b \sin\left(\pi \frac{x - x_0}{x_1 - x_0}\right) \\ &\quad + c \sin^3\left(\pi \frac{x - x_0}{x_1 - x_0}\right) \quad (x_0 \leq x \leq x_1) \\ &= x + a(x + x_0) + b \sin\left(\pi \frac{x + x_0}{x_1 - x_0}\right) \\ &\quad + c \sin^3\left(\pi \frac{x + x_0}{x_1 - x_0}\right) \quad (-x_1 \leq x \leq -x_0) \\ &= x \quad (-x_0 \leq x \leq x_0) \end{aligned} \quad (1)$$

in which $X(x)$ defines the complex coordinate ray X along which the wave function is defined as a function of the real-valued parameter x in which the operators are represented. Smooth scaling occurs between the scaling boundary $x_0 = 4a_0$ and the end of the grid $x_1 \approx 8.78a_0$. The parameters a , b , and c are determined by the scaling angle and stretching factor (half a radian and three, respectively, such that $X'(x) = 4e^{0.5i}$ at $\pm x_1$) and by making the fourth derivative $X''''(x)$ continuous. This transformation defines the new length-gauge dipole operators X , Y , and Z , and the DVR weights in each Cartesian direction (originally uniformly $w_i = \frac{1}{\Delta}$ with Δ the sinc DVR spacing) are modified according to $w_i \rightarrow X'(x_i)w_i$. The first derivative operator matrix elements are transformed as e.g. $(d/dX)_{ij} = (d/dx)_{ij}(X'(x_i)X'(x_j))^{-1/2}$, and the kinetic energy matrix elements are defined in the

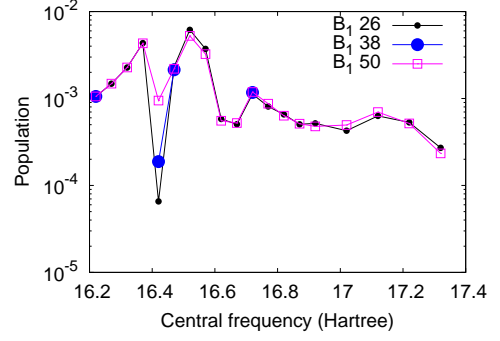


FIG. 1. (Color online) Convergence of the B_1 population at 10^{17} W cm⁻², with respect to the order of the Lebedev quadrature used for the orientation average of fixed-nuclei calculations.

DVR approximation as

$$\left(\frac{\partial^2}{\partial X^2}\right)_{ij} = \frac{1}{X'(x_i)X'(x_j)} \left(\frac{\partial^2}{\partial x^2}\right)_{ij} - \delta_{ij} \frac{3X''(x_i)^2 - 2X'''(x_i)X'(x_i)}{4X'(x_i)^4} \quad (2)$$

We employ a pulse in the dipole approximation with central frequency ω and duration π/Ω as follows. In the velocity gauge we define the vector potential

$$A(t) = \sin^2(\Omega t) \sin\left(\omega \left[t - \frac{\pi}{2\Omega}\right]\right) \quad (0 \leq t \leq \frac{\pi}{\Omega}) \quad (3)$$

In the length gauge we employ the electric field $E(t) = \frac{\partial}{\partial t} A(t)$. The results are gauge-independent on the scale of the figures presented here. For the pulses used here, with 1fs full width at half-maximum (FWHM) in time ($\pi/\Omega = 2$ fs), the FWHM of the spectral profile, the squared Fourier transform $|E_z(\omega)|^2$ is 3.25eV.

We calculate population transfer for the valence B_1 , B_2 , and A_2 states. We integrate the result over orientations using Lebedev quadrature [29–33]. Comparing 38- and 50-point quadrature, we find that most of the results are converged with 38-point quadrature. We have not attempted to demonstrate the convergence of these results beyond 50-point quadrature due to computer resources. In Figure 1 we show the convergence of the B_1 population at 10^{17} W cm⁻², with respect to the order of the Lebedev quadrature.

Due to symmetry, and within the rotating wave approximation, only seven of the 50 points need to be calculated. Each central frequency and intensity required approximately 10,000 cpu-hours to calculate: seven calculations, 121 processors each, and about twelve hours per calculation.

The energies of the valence states are shown in Table I. We provide vertical transition energies from the literature, and also report our transition energies. These are the transition energies of the states used for projection, relative to the initial state used in the MCTDHF propagation. The states are not used in the MCTDHF

	Ref. [35]	Present
B ₁	2.827 eV	4.294 eV
B ₂	3.239 eV	3.850 eV
A ₂	3.977 eV	4.009 eV

TABLE I. Transition energies for valence states: vertical transition energies previously calculated from Ref. [35], and transition energies for states used to define populations from the MCTDHF calculation.

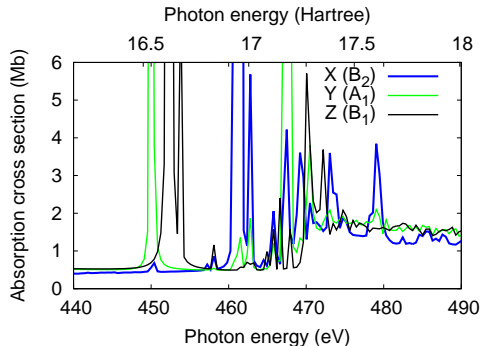


FIG. 2. (Color online) NO₂ photoabsorption cross section calculated in the vicinity of the Oxygen K-edge using a 10fs MCTDHF calculation with a weak pulse. The K-edge is artificially low in these calculations.

calculation, and we have demonstrated [34] that these transition energies do not correspond with transition energies apparent from MCTDHF calculations. They are nevertheless included here for the sake of completeness.

Due to the spacing of sinc functions – again, 0.2975614 bohr – and the fact that we have not elaborated our method with any pseudopotential or effective theory to account for the truncation in momentum space, the core transitions that drive the X-ray Raman process are shifted substantially downward in energy. As can be seen in Fig. 2, the Oxygen K-edge appears at approximately 470eV in these calculations, not the actual 540eV. We expect that the error in the valence population transfer induced by this large shift in the intermediate state transition energy, due to the single-electron discretization, is modest but we have not attempted to quantify it. Because the shift in the Oxygen K-edge means that the Oxygen and Nitrogen K-edges are unphysically close, one would expect that the loss due to ionization of the Nitrogen 1s electron would be enhanced and therefore that the population transfer would be underestimated as a result of this discretization error. However, as discussed below, the cross sections above and below the Oxygen K-edge have the correct magnitude, so the effect of the artificial shift in the Oxygen K-edge may in fact be small.

Fig. 2 shows the photoabsorption cross section calculated in the neighborhood of the Oxygen K-edge. The magnitude of the cross section above and below the edge

(about 0.5 and a bit more than 1.0 respectively) agree well with figure 5.10 in Berkowitz’s compilation [36]. The three peaks at about 450 (*A*₁), and 452 & 453 (*B*₁) correspond to excitations to 6*a*₁ and 2*b*₁ from the Oxygen 1s σ_g orbital, and correspond with the peaks observed at approximately 530, 532, and 533 in experiment [37–39]. Relative to these peaks, there is also a pair of *B*₂ states, at about 462eV, both spin couplings for excitation to 5*b*₂, and the K-edge lies at about 468eV. It is clear that the K-edge is too high in energy, and the *B*₂ states are too low, because the *B*₂ states are observed as a broad core-excited shape resonance in experiment. Experiment [37–39] gives a *A*₁ to *B*₂ excitation energy of 15eV, and a K-edge about 12eV above *A*₁; here they are found at about 12 and 18eV, respectively.

III. RESULTS FOR IMPULSIVE X-RAY RAMAN EXCITATION OF NO₂

The results for population transfer using 1fs FWHM linearly polarized pulses per Eq. 3 are shown in Figure 3.

The best population transfer is obtained for the *B*₁ state, at approximately 3×10^{17} W cm⁻², substantially red-detuned from the second-order optimum. However the optimum population transfer is only 1% with these one-femtosecond, linearly polarized pulses. We will vary chirp and duration in future work.

The second-order behavior is visible in Fig. 3 in the bold black line with open squares, corresponding to intensity 1×10^{15} W cm⁻². This result has been multiplied by 100 in the figure, and lies on top of the orange (grey) line with solid squares in the figure, the line corresponding to intensity 1×10^{16} W cm⁻², on the left-hand side of the figure at lower central frequency. Thus, one can see that even at 1×10^{16} W cm⁻², when the central frequency is low such that the pulse is not resonant with any of the near-edge fine structure nor the continuum above the edge, the behavior is still second-order.

However, as the intensity is increased, strong nonlinear effects arise that are contrary to the conventional wisdom. We see here that the optimum population transfer is obtained with central frequency much different from the the second-order optimum. In Fig. 3, we see that as the intensity is increased, a strong minimum in the population transfer for the *B*₁ and *A*₂ states develops around 447eV in these calculations. This minimum persists for a range of intensities. Among the calculations we have performed, the overall optimum population transfer is seen to occur to the *B*₁ state, below this robust minimum, at 3.16×10^{17} W cm⁻², and a central frequency of 444eV in these calculations. 444eV is approximately 6eV below the lowest state responsible for the near-edge fine structure, the *A*₁ excitation $1s \rightarrow 6a_1$, and 8eV below the 2nd order optimum.

It seems likely from the results that this excitation is driven by nonresonant Raman via the $1s^{-1}$ continuum. For each of the three states, the excitation probability

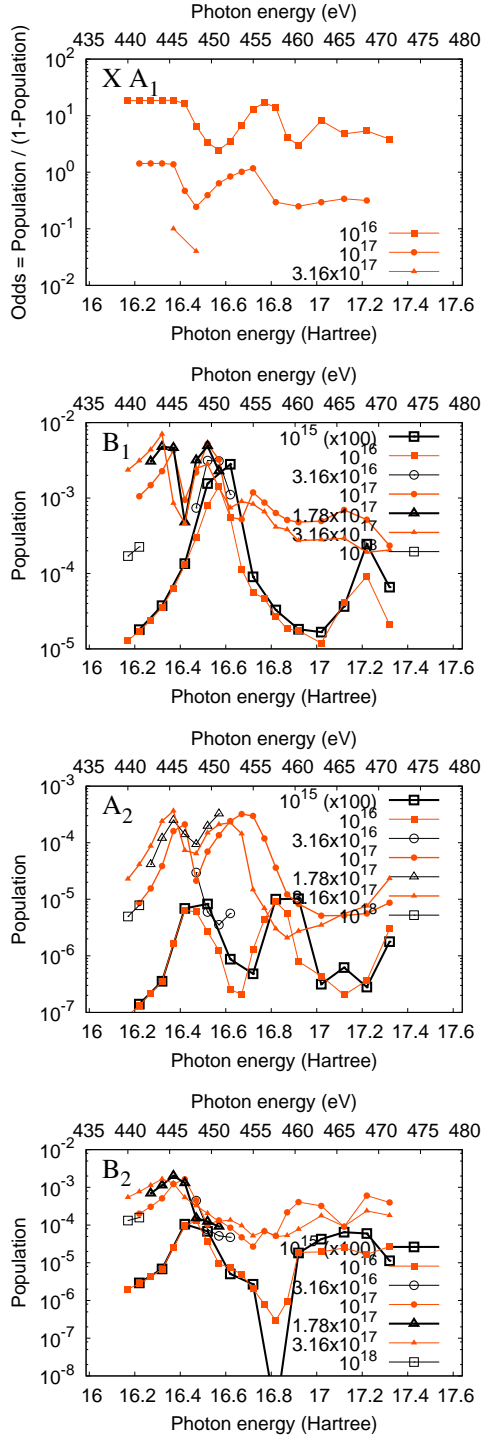


FIG. 3. (Color online) Results for population transfer to the B_1 , A_2 , and B_2 valence excited states of NO_2 , and odds for remaining in the ground state, averaged over orientation, for 1fs pulses, as labeled. Different intensities are plotted with different lines and labeled in Watts per square centimeter.

drops steeply as the central frequency is decreased on the left side of the figures. This behavior is what we would expect from nonresonant Raman, due to increasing red-detuning as the frequency is lowered. In contrast, if population transfer were occurring via direct, resonant, one-electron Raman – via the continuum excitations of the $2s$ or $2p$ electron(s) or the $1s$ electrons of Nitrogen – we would expect relatively constant behavior on the left side of the figure. Furthermore, there is much more oscillator strength available via Oxygen $1s$ excitations to the the continuum than there is via the near-edge fine structure, and therefore nonresonant transitions that are substantially detuned from both the continuum and near-edge fine structure are likely to proceed via the continuum. We plan further calculations and modeling to interrogate the nature of this excitation.

IV. CONCLUSION

The MCTDHF method allows nonlinear processes to be studied at the limits of intensity without making any assumptions about the degree of excitation, ionization, or correlation of the wave function. Using an implementation of the MCTDHF method which is in principle of calculating an accurate solution to the Schrodinger equation including all nonrelativistic electronic effects for polyatomic molecules, we have provided a survey of population transfer to valence electronic states in NO_2 by linearly polarized 1fs pulses tuned near the Oxygen K-edge. Such impulsive x-ray Raman transitions underly proposed methods of multidimensional x-ray Raman spectroscopies [1, 2], and x-ray pulses of the required coherence, synchronization, and intensity will soon be available with developments in next-generation light sources or high harmonic generation.

Most theoretical and computational treatments so far have not considered continuum oscillator strength that may drive the process, and many have been perturbative treatments that explicitly compute only the n th-order response. Our MCTDHF results indicate that in order to drive significant (10^{-3} or more) population transfer in the NO_2 molecule using 1fs pulses, higher-than-2nd-order effects will be encountered at modest intensity ($10^{16} \text{ W cm}^{-2}$).

Furthermore, second order perturbation theory is not a useful tool for determining the conditions for maximum population transfer. Population transfer occurs at a central frequency that is far red-detuned from the optimum at 2nd order. We find that the maximum population transfer occurs 8eV red-detuned from the 2nd order optimum and 6eV red-detuned from any near-edge fine structure, at approximately $3 \times 10^{17} \text{ W cm}^{-2}$. It appears to proceed via nonresonant Raman via the K-edge continuum.

These active-electron calculations on impulsive Raman transitions in a polyatomic molecule will hopefully help guide the selection of experimental conditions under

which multidimensional X-ray spectroscopies are most viable. These calculations are the first step toward first-principles calculations of multidimensional x-ray Raman spectroscopies on polyatomic molecules.

V. ACKNOWLEDGMENTS

Calculations have been performed on the Lawrence Livermore supercluster at Lawrence Berkeley National Laboratory (LBNL) under the support of the Laboratory Research Computing program, <http://scs.lbl.gov>. Some work was performed at Lawrence Berkeley National Laboratory, supported by the US Department of Energy Office of Basic Energy Sciences, Division of Chemical Sciences Contract DE-AC02-05CH11231. Further support was provided by the Peder Sather Grant program.

-
- [1] J. D. Biggs, Y. Zhang, D. Healton, and S. Mukamel, *The Journal of Chemical Physics* **136**, 174117 (2012).
 - [2] S. Mukamel, D. Healton, Y. Zhang, and J. D. Biggs, *Ann. Rev. Phys. Chem.* **64**, 101 (2013).
 - [3] J. D. Biggs, Y. Zhang, D. Healton, and S. Mukamel, *The Journal of Chemical Physics* **138**, 144303 (2013), <http://dx.doi.org/10.1063/1.4799166>.
 - [4] J. D. Biggs, Y. Zhang, D. Healton, and S. Mukamel, *Proceedings of the National Academy of Sciences* **110**, 15597 (2013).
 - [5] A. Kirrander, K. Saita, and D. V. Shalashilin, *Journal of Chemical Theory and Computation* **12**, 957 (2016), pMID: 26717255, <http://dx.doi.org/10.1021/acs.jctc.5b01042>.
 - [6] S. Miyabe and P. Bucksbaum, *Phys. Rev. Lett.* **114**, 143005 (2015).
 - [7] D. J. Haxton, K. V. Lawler, and C. W. McCurdy, *Phys. Rev. A* **83**, 063416 (2011).
 - [8] D. J. Haxton and C. W. McCurdy, *Phys. Rev. A* **91**, 012509 (2015).
 - [9] J. R. Jones, F.-H. Rouet, K. V. Lawler, E. Vecharynski, K. Z. Ibrahim, S. Williams, B. Abeln, C. Yang, W. McCurdy, D. J. Haxton, X. S. Li, and T. N. Rescigno, *Molecular Physics* **114**, 2014 (2016), <http://dx.doi.org/10.1080/00268976.2016.1176262>.
 - [10] D. J. Haxton, C. W. McCurdy, T. N. Rescigno, K. V. Lawler, J. Jones, B. Abeln, and X. Li, LBNL-AMO-MCTDHF.
 - [11] M. Kitzler, J. Zanghellini, C. Jungreuthmayer, M. Smits, A. Scrinzi, and T. Brabec, *Phys. Rev. A* **70**, 041401 (2004).
 - [12] T. Kato and H. Kono, *Chem. Phys. Lett.* **392**, 533 (2004).
 - [13] J. Caillat, J. Zanghellini, M. Kitzler, O. Koch, W. Kreuzer, and A. Scrinzi, *Phys. Rev. A* **71**, 012712 (2005).
 - [14] M. Nest, T. Klamroth, and P. Saalfrank, *J. Chem. Phys.* **122**, 124102 (2005).
 - [15] O. E. Alon, A. I. Streltsov, and L. S. Cederbaum, *J. Chem. Phys.* **127**, 154103 (2007).
 - [16] M. Nest, R. Padmanaban, and P. Saalfrank, *J. Chem. Phys.* **126**, 214106 (2007).
 - [17] M. Nest, F. Remacle, and R. D. Levine, *New J. Phys.* **10**, 025019 (2008).
 - [18] T. Kato and H. Kono, *J. Chem. Phys.* **128**, 184102 (2008).
 - [19] M. Nest, *Chem. Phys. Lett.* **472**, 171 (2009).
 - [20] T. Kato and K. Yamanouchi, *J. Chem. Phys.* **131**, 164118 (2009).
 - [21] T. Kato, H. Kono, M. Kanno, Y. Fujimura, and K. Yamanouchi, *Laser Physics* **19**, 1712 (2009).
 - [22] H. Miyake and L. A. L. D. Jensen, *Phys. Rev. A* **87**, 062511 (2013).
 - [23] T. Sato and K. L. Ishikawa, *Phys. Rev. A* **88**, 023402 (2013).
 - [24] T. Sato and K. L. Ishikawa, *Phys. Rev. A* **91**, 023417 (2015).
 - [25] R. Sawada, T. Sato, and K. L. Ishikawa, *Phys. Rev. A* **93**, 023434 (2016).
 - [26] J. Broeckhove, L. Lathouwers, E. Kesteloot, and P. V. Leuven, *Chem. Phys. Lett.* **149**, 547 (1988).
 - [27] K. Ohta, *Phys. Rev. A* **70**, 022503 (2004).
 - [28] B. Simon, *Physics Letters A* **71**, 211 (1979).
 - [29] V. I. Lebedev, *Zh. Vychisl. Mat. mat. Fiz.* **15**, 48 (1975).
 - [30] V. I. Lebedev, *Zh. Vychisl. Mat. mat. Fiz.* **16**, 293 (1976).
 - [31] V. I. Lebedev, *Sibirsk. Mat. Zh.* **18**, 132 (1977).
 - [32] V. I. Lebedev and A. L. Skorokhodov, *Dokl. Math* **45**, 587 (1992).
 - [33] V. I. Lebedev and D. N. Laikov, *Dokl. Math* **59**, 477 (1999).
 - [34] D. J. Haxton, K. V. Lawler, and C. W. McCurdy, *Phys. Rev. A* **86**, 013406 (2012).
 - [35] N. Wu and X. Chen, *The Journal of Physical Chemistry A* **116**, 6894 (2012).
 - [36] J. Berkowitz, in *Atomic and Molecular Photoabsorption*, edited by J. Berkowitz (Academic Press, London, 2002) pp. 237 – 316.
 - [37] A. Jurgensen and R. G. Cavell, *Chemical Physics* **257**, 123 (2000).
 - [38] T. Gejo, Y. Takata, T. Hatsui, M. Nagasono, H. Oji, N. Kosugi, and E. Shigemasa, *Chemical Physics* **289**, 15 (2003), decay Processes in Core-excited Species.
 - [39] M. Piancastelli, V. Carravetta, I. Hjelte, A. D. Fanis, K. Okada, N. Saito, M. Kitajima, H. Tanaka, and K. Ueda, *Chemical Physics Letters* **399**, 426 (2004).

